replication through an S phase checkpoint to provide time for repair. The ATM-dependent pathway plays an important role in the S phase checkpoint response following ionizing radiation. Stronger S checkpoint activity in irradiated Ku80-null cells is due to the higher ATM kinase activity. Ku affects the ATM-dependent S phase checkpoint following ionizing radiation (Zhou et al., 2002). Ionizing radiation exposure results in the upregulation of Ku70 via a p53/ATM-dependent mechanism. Increased oxidative stress has been reported in neuronal tissues of ATM-deficient mice (Kamsler, Daily, Hochman, Stern, & Shiloh, 2001). It is not clear whether ATM itself is directly involved in sensing the increase in ROS or whether oxidative stress in AT cells is associated with unrepaired DSBs continuously present in the DNA. Transfecting AT cells with the full-length ATM gene assures cell death prevention, which may be assisted by the activation of Ku in response to oxidative stress (Lee, Kim, Morio, & Kim, 2006). ATM may be essential for Ku activation in the process of repairing DNA damage and preventing cell death.

2.4. ATM and Artemis

Artemis was originally identified as deficient in human radiosensitive severe combined immunodeficiency syndrome. Artemis exhibits an intrinsic single strand-specific 5′ to 3′ exonuclease activity and has hairpin-opening endonuclease activity, which is induced by phosphorylation by DNA-PK. Artemis has roles in V(D)J recombination, NHEJ, and regulation of the DNA damage-induced G2/M cell cycle checkpoint. Cells with mutations in the Artemis gene and Artemis-deficient cells exhibit radiosensitivity and defective V(D)J recombination, implicating the Artemis function in NHEJ (Wang et al., 2005). Since the NHEJ reaction functions as a genomic caretaker, particularly in the prevention of translocations and telomere fusions, Artemis deficiency may be related to carcinogenesis.

The *bona fide* phosphorylation sites and physiological relevance of the phosphorylation are, however, still under investigation. Three basic phosphorylation sites (S385, S516/518) and 11 DNA-PK phosphorylation sites were identified by proteomic analysis using matrix-assisted laser desorption/ionization-time of flight mass spectrometry (MALDI-TOF MS). There were nine other putative DNA-PK/ATM phosphorylation sites identified. Most of the phosphorylation sites are clustered in the C-terminus region. It is now evident that Artemis is a downstream component of the ATM signaling pathway; ATM is the major kinase responsible for the modification of Artemis (Poinsignon et al., 2004; Riballo et al., 2004; Zhang et al., 2004). One of the target sites of ATM is S645 of Artemis, and its phosphorylation leads to hyperphosphorylation of Artemis. Artemis phosphorylation by ATM is important in association with the M/R/N complex and Cdk1-cyclin B activation, which in turn controls G2/M checkpoint recovery. On the other hand, phosphatase-treated mammalian Artemis still retains endonuclease activity. Artemis molecule lacking the C-terminal domain is sufficient to complement V(D)J recombination in Artemis-null cells. How endonuclease activity of Artemis and its association with the damaged termini are controlled is still controversial. DNA-PK, ATM, and other not-yet-identified kinase(s) could be involved in the pathway leading to Artemis activation.

3. Cascades

As for DSBs, ATM phosphorylates key proteins in the salvage pathways leading to DSB repair and activation of cell cycle checkpoints (Fig. 1). DNA repair proteins interact with other molecules to repair the damaged DNA through NHEJ or homologous recombination (HR). For instance, ATM phosphorylates key proteins (Ku70/80 and Artemis) to repair the damaged DNA by NHEJ. On the other hand, ATM temporarily arrests the cell cycle by phosphorylating CHK2, which in turn phosphorylates p53, while the damage is being repaired. ATM repairs the damaged DNA through HR by interacting with ATR and the M/R/N complex. When the attempt to repair the

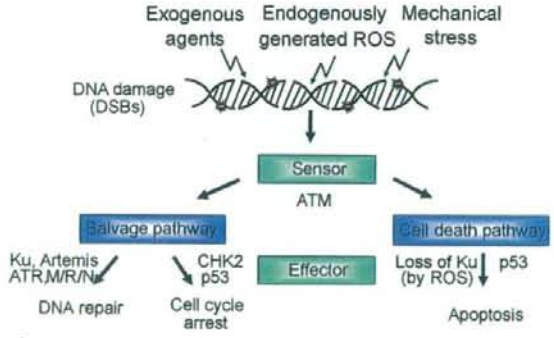

Fig. 1. Cell responses to DNA damage. Upon the formation of DSBs, ATM serves as a sensor for DNA damage and phosphorylates key proteins in pathways leading to DSB repair or the activation of cell cycle checkpoints. ATM phosphorylates key proteins (Ku70/80, Artemis) to repair the damaged DNA. Additionally, ATM temporarily arrests the cell cycle by phosphorylating CHK2, which in turn phosphorylates p53, while the damage is being repaired. ATM repairs the damaged DNA through HR by interacting with ATR and the M/R/N complex. When the attempt to repair the damage fails, the cell undergoes apoptosis via the p53 pathway. Oxidative stress-induced cell death stems from the nuclear loss of Ku70/80.

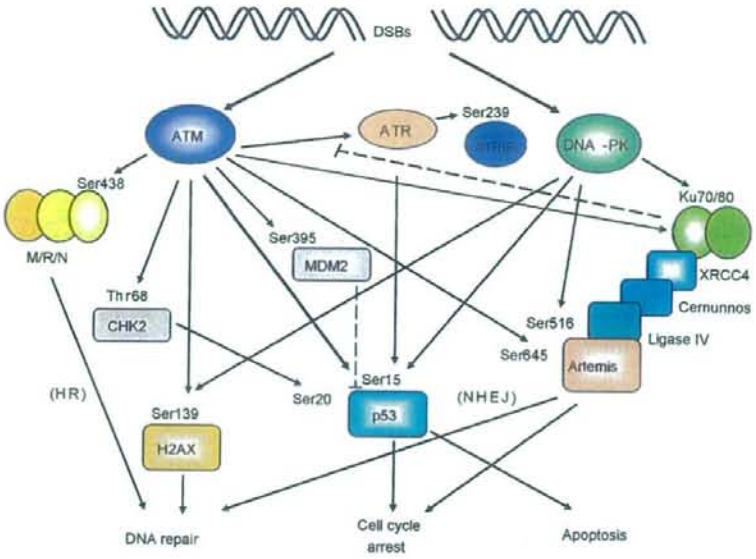

Fig. 2. Targets for the ATM/DNA-PK phosphorylation and signaling network. DNA-PK, ATM, and ATR are recruited to the sites of DNA damage through analogous mechanisms involving conserved interaction motifs observed in Ku80, NBS1, and ATRIP, respectively. Ku70/80 and Artemis play critical roles in the repair of damaged DNA through NHEJ by interacting with XRCC4/Cernunnos/DNA ligase IV. Phosphorylation of Ku70/80 and Artemis by DNA-PK and ATM controls cell cycle arrest and the DNA repair function. ATM triggers the repair of damaged DNA through HR by interacting with the M/R/N complex. ATM phosphorylates CHK2, which phosphorylates p53 to arrest the cell cycle, while damage is being repaired. When the attempt to repair the damage fails, the cell undergoes apoptosis via the p53 pathway. Dotted lines: Ku70/80 also affects ATM-dependent ATR activation. The stability of p53 is also tightly controlled by MDM2.

damage fails, the cell undergoes apoptosis via the p53 pathway. Oxidative stress-induced cell death stems from the nuclear loss of Ku70/80 (Song et al., 2003).

As shown in Fig. 2, DNA repair is mediated by DNA damage response molecules and involves three members of the phosphoinositide-3-kinase-like family (ATM, ATR, and DNA-PK). DNA-PK, ATM, and ATR are recruited to the sites of DNA damage through analogous mechanisms involving conserved interaction motifs observed in Ku80, NBS1, and ATRIP, respectively. The DNA-PK/Ku70/80 complex is required for the NHEJ DNA repair pathway. Artemis plays a role in processing the DNA ends prior to ligation. XRCC4/Cernunnos/DNA ligase IV is recruited to the DNA-PK/Ku complex, which is required for end joining. ATM plays a role in DNA DSB repair in concert with the M/R/N complex. DNA-PK and ATM share several substrates as phosphorylation targets, including Artemis, p53, and histone H2AX. Interplays among Ku70/80, Artemis, DNA-PK, and ATM are involved in DNA damage responses. Ku70/80 also affects ATM-dependent ATR activation. Degradation of key signaling molecules (p53, Ku70/80, and Artemis) is one of the mechanisms determining cell fate. Oxidative stress-induced degradation of Ku70/80 is mediated by caspase-3 (Song et al., 2003). Activity of p53 is regulated by the ubiquitin–proteasome system, which is the major non-lysosymal system for degrading proteins in the cell (Thompson et al., 2007). It is still unclear whether Ku70/80 and Artemis are similarly regulated by proteasome-dependent degradation or other protease systems. Degradation of Ku70/80 leads to upregulation of p53, resulting in apoptosis. The stability of p53 is also tightly controlled by mouse double minute 2 (MDM2) (Fig. 2).

4. Associated pathologies and therapeutic implications

Nuclear loss of Ku70/80 and DNA damage linked to oxidative stress in pancreatic acinar cells has been suggested as pathophysiologic mechanisms of pancreatitis (Song et al., 2003). DNA-PK deficiency in cultured neurons causes an accumulation of DNA damage and increased susceptibility to apoptosis (Chechlacz, Vemuri, & Naegele, 2001). Diminished DNA DSB repair by NHEJ causes a progressive loss of haematopoietic stem cells and bone marrow cellularity during aging (Nijnik et al., 2007). Therefore, the loss of function of Ku proteins and DNA-PK activity might be one of

the important pathological mechanisms in apoptotic cell death related to pancreatic inflammation, neurological disorders, and aging. Since ATM is essential for nuclear Ku activation, maintenance of Ku70/80 and DNA-PK together with ATM may prevent DNA damage in various diseases and inflammation. Artemis serves as a tumor suppressor and patients with hypomorphic mutations in Artemis have a predisposition to develop lymphoma (Moshous et al., 2003). Phosphorylation and degradation of Artemis may be a key step in controlling cellular apoptosis and carcinogenesis. The formation of carcinogenic translocations requires the illegitimate joining of chromosomes containing DSBs. The molecules presented in this review are critical in DNA repair, and their defective function, improper localization, and loss may lead to unrepaired DNA DSBs and to the malignant transformation of cells when they escape apoptosis. The manipulation of these DNA damage response molecules could lead to anti-inflammatory agents and anti-cancer agents.

Acknowledgements

This study was supported by a grant (Joint Research Project under the Korea-Japan Basic Scientific Cooperation Program) from the Korea Science and Engineering Foundation (F01-2006-000-10063-0) (to H. Kim) and from JSPS (to T. Morio). H. Kim is grateful to the Brain Korea 21 Project, Yonsei University.

References

Arrington, E. D., Caldwell, M. C., Kumaravel, T. S., Lohani, A., Joshi, A., Evans, M. K., et al. (2000). Enhanced sensitivity and long-term G2 arrest in hydrogen peroxide-treated Ku80-null cells are unrelated to DNA repair defects. *Free Rad. Biol. Med., 29*, 1166–1176.

Chechlacz, M., Vemuri, M. C., & Naegele, J. R. (2001). Role of DNA-dependent protein kinase in neuronal survival. *J. Neurochem., 78*, 141–154.

Difilippantonio, M. J., Zhu, J., Chen, H. T., Meffre, E., Nussenzweig, M. C., Max, E. E., et al. (2000). DNA repair protein Ku80 suppresses chromosomal aberrations and malignant transformation. *Nature, 404*, 823–825.

Gu, Y., Jin, S., Gao, Y., Weaver, D. T., & Alt, F. W. (1997). Ku70-deficient embryonic stem cells have increased ionizing radiosensitivity, defective DNA end-binding activity, and inability to support V(D)J recombination. *Proc. Natl. Acad. Sci. U.S.A., 94*, 8076–8081.

Kamsler, A., Daily, D., Hochman, A., Stern, N., & Shiloh, Y. (2001). Increased oxidative stress in ataxia telangiectasia evidenced by alterations in redox state of brains from Atm-deficient mice. *Cancer Res., 61*, 1849–1854.

Lee, J. H., Kim, K. H., Morio, T., & Kim, H. (2006). Ataxia-telangiectasia-mutated-dependent activation of Ku in human fibroblasts exposed to hydrogen peroxide. *Ann. N.Y. Acad. Sci., 1090*, 542–548.

Li, Y., Yokota, T., Gama, V., Yoshida, T., Gomez, J. A., Ishikawa, K., et al. (2007). Bax-inhibiting peptide protects cells from polyglutamine toxicity caused by Ku70 acetylation. *Cell Death Differ., 14*, 2058–2067.

Martinez, J. J., Seveau, S., Veiga, E., Matsuyama, S., & Cossart, P. (2005). Ku70, a component of DNA-dependent protein kinase, is a mammalian receptor for *Rickettsia conorii*. *Cell, 12*, 1013–1023.

Morio, T., Hanissian, S. H., Bacharier, L. B., Teraoka, H., Nonoyama, S., Seki, M., et al. (1999). Ku in the cytoplasm associates with CD40 in human B cells and translocates into the nucleus following incubation with IL-4 and anti-CD40 mAb. *Immunity, 11*, 339–348.

Moshous, D., Pannetier, C., Chasseval, R. R., Deist, F. F., Cavazzana-Calvo, M., Romana, S., et al. (2003). Partial T and B lymphocyte immunodeficiency and predisposition to lymphoma in patients with hypomorphic mutations in Artemis. *J. Clin. Invest., 111*, 381–387.

Nijnik, A., Woodbine, L., Marchetti, C., Dawson, S., Lambe, T., Liu, C., et al. (2007). DNArepair is limiting for haematopoietic stem cells during ageing. *Nature, 447*(7145), 686–690.

Poinsignon, C., de Chasseval, R., Soubeyrand, S., Moshous, D., Fischer, A., Hache, R. J., & de Villartay, J. P. (2004). Phosphorylation of Artemis following irradiation-induced DNA damage. *Eur. J. Immunol., 34*, 3146–3155.

Riballo, E., Kuhne, M., Rief, N., Doherty, A., Smith, G. C., Recio, M. J., et al. (2004). A pathway of double-strand break rejoining dependent upon ATM, Artemis, and proteins locating to gamma-H2AX foci. *Mol. Cell, 16*, 715–724.

Shackelford, D. A., Tobaru, T., Zhang, S., & Zivin, J. A. (1999). Changes in expression of the DNA repair protein complex DNA-dependent protein kinase after ischemia and reperfusion. *J. Neurosci., 19*, 4727–4738.

Song, J. Y., Lim, J. W., Kim, H., Morio, T., & Kim, K. H. (2003). Oxidative stress induces nuclear loss of DNA repair proteins, Ku70 and Ku80, and apoptosis in pancreatic acinar AR42J cells. *J. Biol. Chem., 278*, 36676–36687.

Thompson, S. J., Loftus, L. T., Ashley, M. D., & Meller, R. (2007). Ubiquitin–proteasome system as a modulator of cell fate. *Curr Opin Pharmacol.*, on-line publication [Epub ahead of print].

Tomimatsu, N., Tahimic, C. G., Otsuki, A., Burma, S., Fukuhara, A., Sato, K., et al. (2007). Ku70/80 modulates ATM and ATR signaling pathways in response to DNA double strand breaks. *J. Biol. Chem., 282*, 10138–10145.

Wang, J., Pluth, J. M., Cooper, P. K., Cowan, M. J., Chen, D. J., & Yannone, S. M. (2005). Artemis deficiency confers a DNA double-strand break repair defect and Artemis phosphorylation status is altered by DNA damage and cell cycle progression. *DNA Repair (Amst), 4*(5), 556–570.

Zhang, X., Succi, J., Feng, Z., Prithivirajsingh, S., Stpry, M. D., & Legerski, R. J. (2004). Artemis is a phosphorylation target of ATM and ATR and is involved in the G2/M DNA damage checkpoint response. *Mol. Cell Biol., 24*, 9207–9220.

Zhou, X. Y., Wang, X., Wang, H., Chen, D. J., Li, G. C., Iliakis, G., & Wang, Y. (2002). Ku affects the ATM-dependent S phase checkpoint following ionizing radiation. *Oncogene, 21*, 6377–6381.

Int J Hematol (2008) 87:88–90
DOI 10.1007/s12185-007-0017-8

CASE REPORT

Successful treatment of chronic granulomatous disease with fludarabine-based reduced-intensity conditioning and unrelated bone marrow transplantation

Daiichiro Hasegawa · Masako Fukushima · Yuki Hosokawa · Hiroki Takeda · Keiichiro Kawasaki · Tomoyuki Mizukami · Hiroyuki Nunoi · Hiroshi Ochiai · Tomohiro Morio · Yoshiyuki Kosaka

Received: 25 May 2007 / Revised: 27 August 2007 / Accepted: 21 September 2007 / Published online: 7 December 2007

Abstract Allogeneic hematopoietic stem-cell transplantation (HSCT) for chronic granulomatous disease (CGD) with a reduced-intensity conditioning regimen can be expected to lead to less therapy-related mortality and late-onset impairment, whereas it has also been reported to increase the risk of unsustained mixed donor chimerism and late rejection after transplantation. Herein, we report a 4-year-old boy with CGD who was successfully treated with unrelated bone marrow transplantation with a reduced-intensity conditioning regimen (RIC). Fludarabine-based RIC, 4 Gy of total body irradiation, 120 mg/kg of cyclophosphamide, and 125 mg/m^2 of fludarabine, was adopted for transplantation, followed with 8.9×10^8/kg mononucleated donor cells infused without T-cell depletion. Although hematopoietic engraftment was rapidly obtained by day +17, he developed unstable donor chimerism. After tacrolimus withdrawal, the patient showed grade III acute graft-versus-host disease (GVHD), and subsequently reached full donor chimerism by day +61. Twelve months post-transplant, the patient has remained well with stable and durable engraftment, 100% donor chimerism, and normal superoxide production, without the requirement of donor lymphocyte infusions (DLI).

Keywords Chronic granulomatous disease · Unrelated bone marrow transplantation · Reduced intensity conditioning

1 Introduction

Chronic granulomatous disease (CGD) is a primary immunodeficiency caused by impaired phagocyte killing of intracellular pathogens, characterized by recurrent, often life-threatening bacterial and fungal infections and by granuloma formation in vital organs. It results from mutation in any one of four subunits of a nicotinamide adenine dinucleotide phosphate oxidase of phagocytic cells ($gp91^{phox}$, $p47^{phox}$, $p67^{phox}$, and $p22^{phox}$) [1]. Although the prognosis of CGD has markedly improved due to prophylactic treatment for infections, including the induction of interferon-gamma therapy, annual mortality is still between 2 and 5% [2]. Allogeneic hematopoietic stem-cell transplantation (HSCT) is an alternative to conventional treatment for CGD, but a high transplantation-related mortality rate [3] and high risk of graft rejection have lowered its therapeutic efficacy [4]. We here in report a 4-year-old boy with CGD who was successfully treated with unrelated bone marrow transplantation with a fludarabine-based reduced-intensity conditioning regimen (RIC).

2 Case report

A 4-year-old boy with CGD was admitted to our hospital in August 2005. He had had recurrent bacterial and fungal infections from early infancy, and CGD was diagnosed by

D. Hasegawa (✉) · M. Fukushima · Y. Hosokawa · H. Takeda · K. Kawasaki · Y. Kosaka
Department of Hematology and Oncology, Kobe Children's Hospital, 1-1-1 Takakuradai, Suma, Kobe 654-0081, Japan
e-mail: hasegawa_kch@hp.pref.hyogo.jp

T. Mizukami · H. Nunoi
Department of Pediatrics, Miyazaki University School of Medicine, Miyazaki, Japan

H. Ochiai · T. Morio
Center for cell therapy, Tokyo Medical and Dental University, Tokyo, Japan

reduced NADPH oxidase (0%), confirmed by $gp91^{phox}$ expression analysis when he was 1 year old. His elder brother was also diagnosed with CGD, and died of fungal pneumonia at the age of 10 years old. There was no HLA-identical HSCT donor in his family. He received anti-infectious prophylaxis consisting of itraconazole and sulfamethoxazole/trimethoprim. Diagnostic imaging at 3 years of age showed intraperitonial granulation tissue formation and hyperplasia of the intestinal tract, resulting from having intussusceptions two times. Interferon gamma therapy had been given for 6 months before transplantation, but subsequently failed. Thus, allogeneic bone marrow transplantation from an HLA-matched volunteer donor was planned.

At 4 years of age, he received allogeneic bone marrow transplantation from an HLA-matched unrelated donor in March 2006. Donor and recipient HLA matching was confirmed by serotyping and molecular typing of the HLA class I and II loci, respectively. We used a RIC for transplantation with total body irradiation at a dose of 2 Gy (days −8 and −7) without use of the gonadal shield, cyclophosphamide at a dose of 60 mg/kg (days −3 and −2) and fludarabine at a dose of 25 mg/m^2 (days −6, −5, −4, −3 and −2), because the patient had been chronically ill, showing intermittent fever and moderate elevation of CRP values, which was thought to be due to chronic enterocolitis. Repeated stool and blood cultures were negative for bacteria and fungi. Just before transplantation, laboratory findings included increased C-reactive protein (2.39 mg/dl) and a normal beta-D-glucan level. Latex agglutination test for serum *Aspergillus* and serum *Candida* antigens were negative.

A cell dose of 8.9×10^8/kg mononucleated cells was infused to the patient without T-cell depletion. GVHD prophylaxis consisted of tacrolimus (0.03 mg/kg/day i.v. continuous infusion from day −1) and short-term methotrexate (10 mg/m^2 i.v. on day +1, 7.5 mg/m^2 i.v. on days +3 and +6). He was also nursed in a high-efficiency, particulate-air-filtered protected environment, and underwent oral gut decontamination. He received *Peumocystis carinii* prophylaxis by sulfamethoxazole/trimethoprim, which was interrupted after transplantation until neutrophil recovery confirmed. Post-transplant regimen also included acyclovir, ursodeoxycholic acid and intravenous immunoglobulin therapy. Chimerism was studied via the analysis of informative microsatellite DNA sequences. The oxidase-positive neutrophils were detected by flow cytometry with the use of a dihydrorhodamine oxidation assay.

During the conditioning therapy for transplantation, prolonged fever rapidly resolved and C-reactive protein values also decreased to within normal ranges. A total of 300 μg/m^2 of granulocyte-colony stimulating factor was commenced on day +5 post-transplant. The patient engrafted rapidly. He achieved an absolute neutrophil count of 0.5×10^9/l by day +17. Chimerism analysis revealed 62.5% donor cell engraftment by day +21, and 39.3% donor cell engraftment additively decreased by day +34, respectively. To achieve complete chimerism, we stopped all immunosuppressants by day +39, because he had no GVHD confirmed at that time. Subsequently, grade III acute GVHD of his skin and gut were clinically confirmed on day +55, followed by full converted donor chimerism and normal superoxidase production by day +61. He was treated again with tacrolimus and 2 mg/kg of prednisolone for GVHD, and all GVHD symptoms disappeared by day +80. Reactivation of his Cytomegalovirus antigenemia was detected on day +65, and treated with ganciclovir with good response. Flow cytometric analysis with the use of a dihidrorhodamine

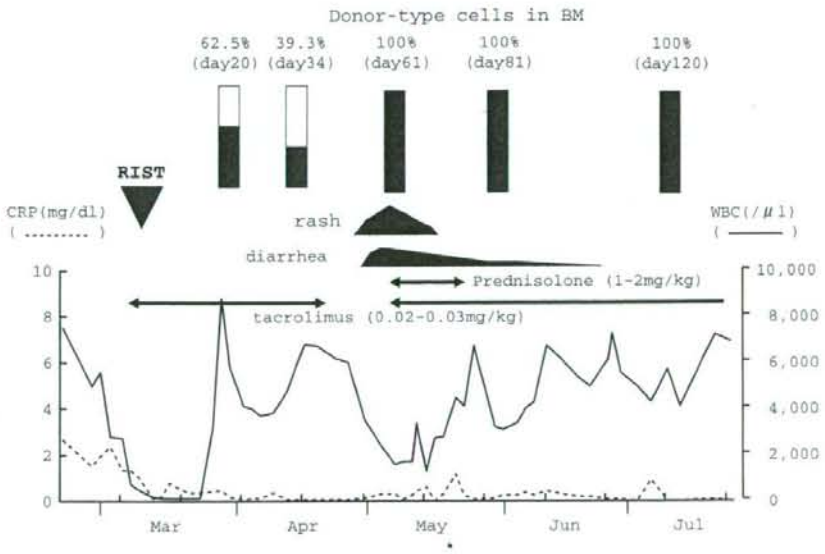

Fig. 1 Clinical course after unrelated bone marrow transplantation. RIST indicates reduced intensity stem cell transplantation. In the upper section of the figure, the donor-type cells in the bone marrow are represented as *black-lacquered*

oxidation assay showed that oxidase-positive neutrophils were detected as 100% of engrafted cells since then. Twelve months post-transplant, the patient has remained well, with stable and durable engraftment, 100% donor chimerism, normal superoxide production, without donor lymphocyte infusion (DLI) requirement (Fig. 1).

3 Discussion

Allogeneic HSCT is the curative therapy for CGD, especially in patients with no inflammatory or infectious lesions at transplant with an excellent disease-free survival rate (DFS). A survey of European Group for blood and marrow transplantation (EBMT) has advocated myeloablative regimens, mostly consisting of busulfan (16 mg/kg) and cyclophosphamide (200 mg/kg), and T-cell replete allografts from HLA-matched related donors, which provided excellent results in low-risk CGD patients (15 children and 1 adult) with no overt infectious complications at transplant and a DFS of 100% [3]. However, in the EBMT report, inadequately high rates of severe acute GVHD and pulmonary infectious complication with a transplant-related mortality of 36% (4 of 11 patients) were also observed in advanced CGD patients with active inflammation due to granulomatous colitis or active infectious disease. Thus, transplant-related mortality with standard myeloablative transplantation regimens, especially in advanced CGD, has been a major obstacle to the more widespread use of allogeneic HSCT.

Horwitz et al. recently reported promising results in the treatment of 10 advanced CGD patients with the combination of a nonmyeloablative regimen consisting of cyclophosphamide, fludarabine, and antithymocyte globulin and the use of a T-cell depleted HLA-identical allograft [5]. This US trial demonstrated that seven out of 10 patients were successfully cured of the disease, even though two patients rejected their graft and DLI led to GVHD in three patients, which was fatal in one case. There are also several reports of successful outcomes for CDG with fludarabine-based RIC [6–9], while most of them consisted of transplant from HLA-matched related donors. Furthermore, T-cell depletion could be a promising approach to reduce the incidence of GVHD, while it could be associated with an increased risk of infectious complications and graft rejection. Thus, RIC is associated with a lower toxity from the conditioning agents and may be an alternative option for CGD, while it still carries a significant risk of graft rejection and GVHD, particularly if DLI have to be used to ensure engraftment.

A national survey of HSCT for CGD in Japan has shown fairly high survival rate (22 of 28), in which the survival rate of HSCT from HLA-matched siblings were comparable to that of HSCT from HLA-matched unrelated donors, whereas that of cord blood transplantation were improperly poor (2 of 4) [10]. Recently, nonmyeloablative conditioning regimens, mostly consisting cyclophosphamide and fludarabine, have been preferred, while the myeloablative conditioning, consisted of busulfan and cyclophosphamide, have been initially performed. However, inadequately high rates of development of unsustained mixed chimerism with the requirement of DLIs were also demonstrated in the patients with RIC by cyclophosphamide and fludarabine. In current case, we adapted fludarabine-based RIC without T-cell deletion for transplantation, because it is not allowed to manipulate unrelated donor allografts for DLIs, and also increased the total body irradiation dose to 4 Gy to ensure engraftment. Taken together, although standard regimens for transplantation of advanced CGD have not been established, our present case encourages the consideration of unrelated HSCT with fludarabine-based RIC for patients with CGD, even if they have infectious complications and no suitable related donors.

References

1. Lekstrom-Himes JA, Gallin JI. Advances in immunology: immunodeficiency diseases caused by defects in phagocytes. N Engl J Med. 2000;343:1703–4.
2. Winkelstein JA, Marino MC, Johnston RB Jr, et al. Chronic granulomatous disease. Report on a national registry of 368 patients. Medicine. 2000;79(3):155–9.
3. Seger RA, Gungor T, Belohradsky BH, et al. Treatment of chronic granulomatous disease with myeloablative conditioning and an unmodified hemopoietic allograft: a survey of the European experience, 1985–2000. Blood. 2002;100(13):4344–50.
4. Nagler A, Ackerstein A, Kapelushnik J, Or R, Naparstek E, Slavin S. Donor lymphocyte infusion post-non-myeloablative allogeneic peripheral blood stem cell transplantation for chronic granulomatous disease. Bone Marrow Transplant. 1999;24(3):339–42.
5. Horwitz ME, Barrett AJ, Brown MR, et al. Treatment of chronic granulomatous disease with nonmyeloablative conditioning and a T-cell-depleted hematopoietic allograft. N Engl J Med. 2001;344(12):881–8.
6. Nicholson JAT, Wynn RF, Carr TF, Will AM, et al. Sequential reduced- and full-intensity allografting using same donor in a child with chronic granulomatous disease and coexistent, significant comorbidity. Bone Marrow Transplant. 2004;34(11):1009–10.
7. Gungor T, Halter J, Klink A, Junge S. Successful low toxicity hematopoietic stem cell transplantation for high-risk adult chronic granulomatous disease patients. Transplantation. 2005;79(11):1596–606.
8. Sastry J, Kakakios A, Tugwell H, Shaw PJ. Allogeneic bone marrow transplantation with reduced intensity conditioning for chronic granulomatous disease complicated by invasive Aspergillus infection. Pediatr Blood Cancer. 2006;47(3):327–9.
9. Kikuta A, Ito M, Mochizuki K, et al. Nonmyeloablative stem cell transplantation for nonmalignant diseases in children with severe organ dysfunction. Bone Marrow Transplant. 2006; 38(10):665–9.
10. Nunoi H. Two breakthroughs in CGD studies. Nihon Rinsho Meneki Gakkai Kaishi. 2007;30(1):1–10.

Reprinted from BRITISH JOURNAL OF OPHTHALMOLOGY, April 2008, Vol 10.1136/bjo.2007.125773, p 505-508

Association of varicella zoster virus load in the aqueous humor with clinical manifestations of anterior uveitis in herpes zoster ophthalmicus and zoster sine herpete

S Kido,[1] S Sugita,[1] S Horie,[1] M Miyanaga,[2] K Miyata,[2] N Shimizu,[3] T Morio,[4] M Mochizuki[1]

[1] Department of Ophthalmology & Visual Science, Tokyo Medical and Dental University, Tokyo, Japan; [2] Miyata Eye Hospital, Miyakonojyo, Japan; [3] Department of Virology, Medical Research Institute, Tokyo Medical and Dental University, Tokyo, Japan; [4] Center for Cell Therapy, Tokyo Medical and Dental University, Tokyo, Japan

Correspondence to:
Dr S Sugita, Department of Ophthalmology & Visual Science, Tokyo Medical and Dental University Graduate School of Medicine, 1-5-45 Yushima, Bunkyo-ku, Tokyo 113-8519, Japan; sunaoph@tmd.ac.jp

Accepted 4 August 2007
Published Online First
1 February 2008

ABSTRACT

Aim: To investigative whether clinical manifestations of anterior uveitis are associated with the viral load of varicella zoster virus (VZV) in the aqueous humor in patients with herpes zoster ophthalmicus (HZO) and zoster sine herpete (ZSH).

Methods: After informed consent was given, an aliquot of aqueous humor was collected from patients with VZV anterior uveitis (n = 8). Genomic DNA of the human herpes viruses was measured in the aqueous humor by two PCR assays: a qualitative multiplex PCR and a quantitative real-time PCR.

Results: All patients had unilateral acute anterior uveitis with high intraocular pressure, mutton fat keratic precipitates with some pigmentation, and trabecular meshwork pigmentation. Multiplex PCR demonstrated VZV genomic DNA in all of the samples, but not in other human herpes virus samples (human simplex virus types 1 and 2, Epstein–Barr virus, cytomegalovirus and human herpes virus types 6, 7 and 8). Real-time PCR revealed a high copy number of VZV DNA in the aqueous humor. After the initial onset of anterior uveitis, iris atrophy and distorted pupil with paralytic mydriasis developed. The intensity of iris atrophy and pupil distortion, but not ocular hypertension, correlated with the viral load of VZV in the aqueous humor.

Conclusion: VZV viral load in the aqueous humor correlated significantly with damage to the iris (iris atrophy and pupil distortion) in patients with HZO and ZSH.

Varicella zoster virus (VZV) affects the first branch of the trigeminal nerve and is known to cause unilateral anterior uveitis (VZV anterior uveitis) characterised by mutton-fat keratic precipitates (KPs), trabecular meshwork pigmentation, ocular hypertension, iris atrophy and distorted pupil. Systemic signs in VZV iridocyclitis can be herpes zoster ophthalmicus (HZO) with skin eruptions or zoster sine herpete (ZSH) without skin eruptions but solely with neuralgia. Using PCR, previous studies have revealed genomic DNA of VZV in the aqueous humor in patients with anterior uveitis with HZO and ZSH.[1 2] Recent advances in molecular biology now make it possible for quantitative measurement of the viral load using real-time PCR. Therefore, this study aimed to quantitatively measure the viral load of VZV in the aqueous humor and analyse the correlation between viral load in the aqueous humor and clinical manifestations of VZV anterior uveitis in patients with HZO and ZSH.

MATERIALS AND METHODS

Subjects

The subjects were eight patients (three men and five women; age range 43–71 years (mean 61)) with diagnosed VZV anterior uveitis at Tokyo Medical and Dental University Hospital and Miyata Hospital between December 1999 and September 2007. The clinical diagnosis of VZV anterior uveitis was based on observation of anterior uveitis associated with either HZO or ZSH. After informed consent had been obtained, an aliquot of aqueous humor (0.1–0.2 ml) was obtained from each patient. The research followed the tenets of the Declaration of Helsinki, and the study was approved by the institutional ethics committees of Tokyo Medical and Dental University.

PCR assay

The aqueous humor samples were centrifuged at 3000 rpm for 5 min and used for the following PCR assays: multiplex PCR and real-time PCR.[3] Multiplex PCR was designed to qualitatively measure the genomic DNA of eight human herpes viruses: herpes simplex virus type 1 (HSV-1) and type 2 (HSV-2), VZV, Epstein–Barr virus (EBV), cytomegalovirus (CMV), human herpes virus type 6 (HHV-6), type 7 (HHV-7) and type 8 (HHV-8). DNA was extracted from the aqueous humor samples using a DNA minikit (Qiagen, Valencia, CA, USA). Multiplex PCR was performed using LightCycler (Roche, Basle, Switzerland). The primer sequences and PCR conditions for VZV were as previously described.[4]

Real-time PCR was performed only for HHV, the genomic DNA of which was detected by multiplex PCR. It was performed by using Amplitaq Gold and a Real-Time PCR 7300 system (ABI, Forster City, CA, USA). The primer sequences for VZV (ORF29) used in real-time PCR were designed to use Primer Express (ABI): forward, AACTTTTACATCCAGCCTGGCG; reverse, GAAAACCCAAACCGTTCTCGAG. The probe was FAM-TGTCTTTCACGGAGGCAAAC-ACGT-TAMRA. The following PCR conditions were used: denaturation at 95°C for 10 min, 95°C for 15 s, and 60°C for 60 s for 40 cycles.

Table 1 Clinical findings at initial presentation in patients with varicella zoster virus (VZV) anterior uveitis

Case	Age (years)	Sex	Eye	Initial ocular findings: VA	IOP (mm Hg)	Mutton-fat KPs	Cells in AC	Flare in AC	Pigmentation in the AC angle	Eruption	Time from onset to treatment	Herpes virus DNA: VZV	Others*
1	67	F	Left	0.3	38	+	3+	271	Wide	–	2 months	+	–
2	70	F	Left	0.3	22	+	3+	106	Partial	+	2 weeks	+	–
3	68	F	Right	0.8	10	+	2+	34	None	–	2 months	+	–
4	56	M	Left	1.2	46	+	3+	241	Partial	+	2 months	+	–
5	70	F	Left	1.2	25	–	1+	13	Partial	–	2 months	+	–
6	44	M	Right	0.6	46	–	3+	140	Partial	+	1 week	+	–
7	43	F	Left	1.2	28	–	2+	15	Partial	–	1 month	+	–
8	71	M	Right	0.3	28	–	2+	13	None	+	None	+	–

Aqueous humor samples from eight cases were analysed for human herpes virus DNA by multiplex PCR.
*Herpes viruses excluding VZV, ie, herpes simplex virus type 1 and type 2, Epstein–Barr virus, cytomegalovirus, human herpes virus types 6, 7 and 8.
VA, visual acuity; IOP, intraocular pressure; KPs, keratic precipitates; AC, anterior chamber.

Statistical analysis

Statistical analysis was performed using the Mann–Whitney U test. Statistical significance was set at $p<0.05$.

RESULTS

Clinical manifestations

In four of the patients, there was an episode of skin eruption with neuralgia in the area of the first branch of the trigeminal nerve; this was clinically diagnosed as HZO (table 1). No skin eruptions were observed in the other patients, although they complained of pain near the first branch of the trigeminal nerve, leading to the diagnosis of ZSH. At various intervals after the onset of HZO or ZSH, the patients developed unilateral anterior uveitis. All patients had cells and flare in the anterior chamber, with increased flare values measured by a laser flare meter (Cowa, Tokyo, Japan). Four patients exhibited mutton-fat KPs (table 1), which had brownish pigmentation and were small or medium in size. Three patients with HZO already exhibited iris atrophy and pupil distortion on referral. High intraocular pressure (IOP) was recorded in all patients except in case 3 (table 1). A gonioscopic examination revealed wide, open angles in all patients, and higher pigmentation in the affected eye than the other eye in six of the eight patients. Ophthalmoscopic examinations revealed no significant inflammatory lesions in the retina and choroid. These clinical results led us to a diagnosis of anterior uveitis associated with HZO or ZSH, with paracentesis subsequently performed in order to carry out the PCR analysis.

After confirmation of the presence of VZV in the aqueous humor by multiplex PCR, systemic anti-VZV agents (aciclovir or valaciclovir) and aciclovir ointment were administered for at least 4 weeks together with a topical corticosteroid (eg, betamethasone) and anti-glaucoma agents (eg, timolol and latanoprost). Iris atrophy and pupil distortion developed during the clinical course (fig 1, table 2). The anterior uveitis and high IOP responded well to treatment.

PCR analysis of the aqueous humor

Qualitative PCR (multiplex PCR) detected genomic DNA of VZV but not of other human herpes viruses (HSV-1, HSV-2, EBV, CMV, HHV-6, HHV-7 and HHV-8) in the aqueous humor of all eight patients (table 1). In peripheral blood samples, however, no genomic DNA of any of the eight human herpes viruses, including VZV, was detected in any of the patients.

Quantitative PCR (real-time PCR) detected significant viral loads of VZV DNA in the aqueous humor of the eight patients ranging from 3.8×10^3 to 1.2×10^7 copies/ml (table 2). It is of note that the VZV viral load in the aqueous humor correlated with the intensity of iris atrophy and pupil distortion (table 2, fig 1). Patient 1 had the highest VZV viral load (1.2×10^7 copies/ml) in the aqueous humor and also had the most severe iris atrophy, with multiple wide areas of segmental iris atrophy and a widely dilated pupil (fig 1A, table 2). Patients 2–5 had the second

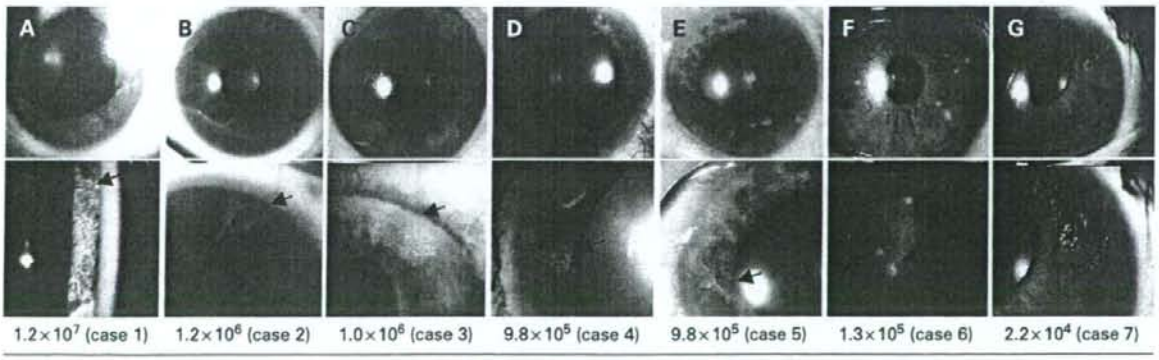

Figure 1 Iris photographs for patients with varicella zoster virus (VZV) anterior uveitis. Slit-lamp photographs are available for seven cases as shown. The numbers indicate the copies of the VZV genomic DNA for each of the aqueous humor samples (copies/ml). Arrows point to areas of iris atrophy. Consent has been obtained for publication of this figure.

Table 2 Virological analysis and ocular findings after treatment of patients with varicella zoster virus (VZV) anterior uveitis

Case	VZV DNA (copies/ml)	Final ocular findings: VA	IOP (mm Hg)	Cells in AC	Flare in AC	Iris atrophy	Extent of iris atrophy (%)	Pupil	Maximum pupil diameter (mm)	Systemic treatment	Follow-up (months)
1	1.2×10^7	mm	10	–	13	Wide	40	Distorted, mydriasis	8.1	ACV, ACZ	48
2	1.2×10^6	0.9	14	–	8	Segmental	4	Distorted, mild mydriasis	3.4	VCV, ACZ	5
3	1.0×10^6	0.8	7	–	5	Segmental	15	Distorted, mydriasis	5.0	VCV	4
4	9.8×10^5	0.9	10	–	73	Segmental	20	Distorted, mydriasis	7.9	VCV	12
5	9.8×10^5	0.8	20	–	22	Segmental	29	Distorted, mydriasis	7.0	VCV	5
6	1.3×10^5	1.5	13	–	6	Circular	1	Normal	2.6	ACV	26
7	2.2×10^4	2	16	–	3	Circular	1	Distorted, mild mydriasis	4.3	VCV	13
8	3.8×10^2	1.2	12	–	9	None	0	Normal	2.6	ACV, ACZ	4

The copy number of the VZV genome in aqueous humor was evaluated with real-time PCR. The extent of iris atrophy was calculated using Photoshop Elements V2.0. ACV, aciclovir; ACZ, acetazolamide; mm, motus manus; VCV, valaciclovir.

highest viral loads in the aqueous humor ($\sim1\times10^6$ copies/ml), and these patients developed multiple segmental or circular iris atrophy with moderate pupil distortion, although these signs were not as marked as in patient 1 (fig 1B–E, table 2). Patients 6 and 7 had the third highest viral load (10^5–10^4 copies/ml) and exhibited circular iris atrophy with minimum pupil distortion (fig 1F,G). Patient 8 had the lowest viral load. This patient exhibited no iris atrophy and the pupil remained normal throughout the clinical course.

We next examined whether higher viral load in the aqueous humor was significantly associated with the intensity of the iris atrophy and pupil distortion. For this analysis, we separated the patients into two groups: higher viral load (patients 1–5) and lower viral load (patients 6–8). The extent of iris atrophy was significantly ($p<0.05$) larger in the group with higher viral load. In addition, the maximum pupil diameter in the pupil distortion was significantly ($p<0.05$) larger in the group with higher viral load. These results suggest that higher viral load in the aqueous humor is closely associated with the intensity of the iris atrophy and pupil distortion.

DISCUSSION

Human herpes viruses are known to be involved in many ocular pathological conditions, such as keratitis, anterior uveitis and necrotising retinitis. Early treatment with anti-viral agents, based on a rapid and accurate diagnosis of the viral infection in ocular tissues, is clinically important in order to avoid the irreversible tissue damage and visual impairment caused by viral infection. Recent advances in PCR methodology have made it possible to screen for viral infection and further quantify the intensity of the viral infection in ocular inflammatory diseases.[1–3 5–8] Asano *et al*[8] detected herpes virus DNA (VZV or HSV-2) in three cases of acute retinal necrosis using real-time PCR. They monitored viral load in ocular samples of these patients and examined correlations with disease activities of acute retinal necrosis. In this study, we used multiplex PCR to screen for HHV infections (HHV1–8) and real-time PCR to quantify viral load in the aqueous humor of patients with HZO or ZSH.

With multiplex PCR, genomic DNA of VZV was detected in the aqueous humor of all eight patients with HZO and ZSH, and significant VZV viral loads were quantified in the same samples with real-time PCR. After cutaneous lesions or neuralgia, all eight patients with HZO or ZSH developed anterior uveitis, which was characterised by unilateral acute anterior uveitis with high IOP, mutton-fat KPs, trabecular meshwork pigmentation, iris atrophy and pupil distortion, although there were no significant pathological lesions in the cornea or ocular fundus of any of the patients. It is well established that these ocular signs are typical of HZO. The present multiplex PCR data clearly confirm that VZV, but not the other human herpes viruses, is responsible for the anterior uveitis. Furthermore, an important finding in our study was that the extent of iris atrophy and pupil distortion also correlated with the viral load of VZV in the aqueous humor in patients with HZO and ZSH. Unlike iris atrophy, IOP did not correlate with the viral load in the aqueous humor. All but one of the patients had raised IOP ranging from 22 to 46 mm Hg at the onset of anterior uveitis.

This study did not reveal any pathological mechanisms for the correlation of the high VZV viral load with the iris atrophy. However, a previous immunohistological report detected VZV antigens in the stroma and vascular endothelial cells of the iris in anterior uveitis patients with HZO.[9] Another study that used angiography in a patient with HZO showed that there was occlusion of the blood vessels of the atrophic iris.[10] On the basis of previous studies and our present data, we hypothesise that the pathological changes caused by VZV may induce occlusion of the iris vessel leading to iris muscle paralysis, with a net result of iris atrophy and pupil distortion. The higher the viral load in the anterior chamber, the more VZVs there will be in the iris, and thus the more intense the pathological tissue damage.

Early initiation of systemic anti-viral agents, as guided by PCR analysis, would help to avoid, or at least minimise, tissue damage in the iris. Some patients with HZO were only given 1-week systemic anti-viral treatments after the onset of the skin lesions. In these patients, the viral loads of VZV in the aqueous humor were high, and various degrees of iris atrophy and distorted pupil were seen over time. These observations suggest that systemic anti-viral treatments after the onset of HZO are helpful in avoiding or minimising irreversible ocular complications and that qualitative and quantitative PCR can also provide useful information for developing treatments for such patients.

Acknowledgements: We thank Drs Ken Watanabe and Miki Mizukami for technical assistance. This work was supported by a Grant-in-Aid for Young Scientists (B) 18791263 from the Ministry of Education, Culture, Sports, Science and Technology, Japan.

Competing interests: None declared.

Ethics approval: Ethics approval was obtained.

Patient consent: Consent has been obtained for publication of fig 1.

REFERENCES

1. **Yamamoto S,** Tada R, Shimomura Y, *et al*. Detecting varicella-zoster virus DNA in iridocyclitis using polymerase chain reaction. *Arch Ophthalmol* 1995;**113**:1358–9.
2. **Nakamura N,** Tanabe M, Yamada Y, *et al*. Zoster sine herpete with bilateral ocular involvement. *Am J Ophthalmol* 2000;**129**:809–10.

3. **Sugita S,** Shimizu N, Kawaguchi T, *et al*. Identification of human herpesvirus 6 in a patient with severe unilateral panuveitis. *Arch Ophthalmol* 2007**125**:1426–7.
4. **Espy MJ,** Teo R, Ross TK, *et al*. Diagnosis of varicella-zoster virus infections in the clinical laboratory by LightCycler PCR. *J Clin Microbiol* 2000;**38**:3187–9.
5. **De Schryver I,** Rozenberg N, Cassoux S, *et al*. Diagnosis and treatment of cytomegalovirus iridocyclitis without retinal necrosis. *Br J Ophthalmol* 2006;**90**:852–5.
6. **Koizumi N,** Yamasaki K, Kawasaki S, *et al*. Cytomegalovirus in aqueous humor from an eye with corneal endotheliitis. *Am J Ophthalmol* 2006;**141**:564–5.
7. **Tran TH,** Rozenberg F, Cassoux N, *et al*. Polymerase chain reaction analysis of aqueous humor samples in necrotising retinitis. *Br J Ophthalmol* 2003;**87**:79–83.
8. **Asano S,** Yoshikawa T, Kimura H, *et al*. Monitoring herpesvirus DNA in three cases of acute retinal necrosis by real-time PCR. *J Clin Virol* 2004;**29**:206–9.
9. **Nakashizuka H,** Yamazaki Y, Tokumaru M, *et al*. Varicella-zoster viral antigen identified in iridocyclitis patient. *Jpn J Ophthalmol* 2002;**46**:70–3.
10. **Marsh RJ,** Easty DL, Jones BR, *et al*. Iritis and iris atrophy in herpes zoster ophthalmicus. *Am J Ophthalmol* 1974;**78**:255–61.

BMJ Publishing Group

BMA House, Tavistock Square, London WC1H 9JR. Tel. 020 7383 6305. Fax. 020 7383 6699

Printed in the UK by Henry Ling Limited, at The Dorset Press, Dorchester DT1 1HD HL/BJO/74/08